UC Irvine
UC Irvine Previously Published Works

Title

Uniform spacing interrogation of a Fourier domain mode-locked fiber Bragg grating sensor system using a polarization-maintaining fiber Sagnac interferometer

Permalink

https://escholarship.org/uc/item/5xj159vs

Journal

Measurement Science and Technology, 24(6)

ISSN

0957-0233

Authors

Lee, Hwi Don
Jung, Eun Joo
Jeong, Myung Yung
et al.

Publication Date

2013-06-01

DOI

10.1088/0957-0233/24/6/065101

Copyright Information

Peer reviewed

Uniform spacing interrogation of a Fourier domain mode-locked fiber Bragg grating sensor system using a polarization-maintaining fiber Sagnac interferometer

Hwi Don Lee[1], **Eun Joo Jung**[2], **Myung Yung Jeong**[1], **Zhongping Chen**[1,3], and **Chang-Seok Kim**[1]

Chang-Seok Kim: ckim@pusan.ac.kr

[1]Department of Cogno-Mechatronics Engineering, World Class University Program, Pusan National University, Busan, 609-735, Korea

[2]Nano-Photonics Research Center, Korea Photonics Technology Institute, Gwangju 500-779, Korea

[3]Beckman Laser Institute, Department of Biomedical Engineering, University of California, Irvine, CA 92612, USA

Abstract

A novel linearized interrogation method is presented for a Fourier domain mode-locked (FDML) fiber Bragg grating (FBG) sensor system. In a high speed regime over several tens of kHz modulations, a sinusoidal wave is available to scan the center wavelength of an FDML wavelength-swept laser, instead of a conventional triangular wave. However, sinusoidal wave modulation suffers from an exaggerated non-uniform wavelength-spacing response in demodulating the time-encoded parameter to the absolute wavelength. In this work, the calibration signal from a polarization-maintaining fiber Sagnac interferometer shares the FDML wavelength-swept laser for FBG sensors to convert the time-encoded FBG signal to the wavelength-encoded uniform-spacing signal.

Keywords

Sagnac interferometer; wavelength-swept laser; fiber Bragg grating

1. Introduction

Fiber Bragg grating (FBG) sensors have many advantages such as resistance to electromagnetic interference, long distance sensing, wavelength selectivity and environmental endurance, and reduced size [1]. Many kinds of interrogation methods have been reported to demodulate FBG signals [2–5]. However, most previous interrogation systems suffered from slow speed below kHz order, which cannot detect a real-time dynamic response of FBG sensors.

Recently, FBG sensor systems with a wavelength-swept laser have been proposed to overcome the interrogation speed limit [6–9]. The development of a higher speed over 10 kHz is crucial for the wide applications of the real-time FBG sensor system, such as for ultra-fast dynamic strain monitoring of fluidic sloshing pressure in a liquefied natural gas carrier tank [10, 11]. In these methods, the time-encoded wavelength scanning light from the wavelength-swept laser is directly related to the interrogation speed. In addition, these methods have many advantages such as high signal to noise ratio and high resolution. However, to provide high sweep Fourier domain mode-locked (FDML) modulation,

wavelength-swept lasers generally have non-uniform spacing scans with respect to wavelength or optical frequency because only sinusoidal waves can be modulated in the regime of several tens of kHz. It is clear that a triangular wave will be suitable for the uniform spacing scan, but the high frequency triangular waves can cause a nonlinearity response and a drop in the capacitance of piezo-electric devices [12]. Thus, sinusoidal excitation is generally used with the piezo-controlled fiber Fabry–Perot tunable filter (FFP-TF) for high frequency resonance operation.

We have reported the first demonstration of an FDML FBG sensor system with four FBG sensors of 1534.1, 1536.7, 1541.8 and 1549.2 nm (see [7]), but only the central wavelength regions (1541.8–1543.3 nm) of scanning can be used for real-time integration of 0–3 mε strain because these center regions show more uniform wavelength spacing compared to other regions. It is evident that when the time-encoded parameter is converted into wavelength, the sinusoidal modulation suffers from an exaggerated, nonuniform wavelength-spacing response around both edge wavelength scanning regions. Therefore, it is critically necessary to compensate for the distorted non-uniform spectrum due to the sinusoidal modulation signal during high speed FBG interrogation. In biomedical imaging, the nonlinearity of wavelength-swept lasers has been studied to interpolate a uniform wavenumber (k) interval [13–15], but no study has been conducted to observe uniform spacing interrogation on FDML FBG sensor systems.

In this study, we suggest a novel and simple method for converting from the time-encoded parameter to the wavelength-encoded parameter of uniform spacing. Using the comb spectral reference of the polarization-maintaining fiber (PMF) Sagnac interferometer, which shares the output of the FDML wavelength-swept laser simultaneously, we achieve the third-order polynomial conversion of the time-encoding to demonstrate the linearized interrogation of the FDML FBG sensor system. The PMF Sagnac interferometer has several advantages, including independence of input polarization [16], discrete tunability of the spectral period [17], reduced temperature sensitivity and low cost compared with the Fabry–Perot type filter [18].

2. Experimental setup and methods

Figure 1 shows the experimental setup for the uniform wavelength spacing of the FBG sensor system with the FDML wavelength-swept laser. The FDML wavelength-swept laser was composed of a semiconductor optical amplifier (SOA from Inphenix Co.), two isolators for a unidirectional ring configuration, a 10 km delay fiber that corresponds to the FDML frequency, an FFP-TF (from Lambda Quest Co.) for selecting the lasing wavelength, a polarization controller (PC) and a 90:10 output coupler. The FFP-TF has a linewidth of 0.25 nm and a free spectral range of 150 nm. This band-pass filter is repeatedly scanned with a sinusoidal wave voltage signal to produce wavelength sweeping in the spectral region of the optical gain. Since the length of the delay fiber is 10 km, we can easily obtain stable and high speed FDML operation for 20.3 kHz wavelength sweeping. The FDML wavelength-swept laser has a broad sweeping bandwidth of 1532–1555 nm. To cover the entire wavelength scanning region, including both the edge wavelength regions of exaggerated, non-uniform wavelength spacing, we intentionally selected the wavelengths of 1534.1, 1544.7, 1549.2 and 1554.0 nm for the four FBGs in the sensor array. All of the FBGs displayed a high reflectivity of more than 90% and a narrow 3 dB bandwidth of ~0.2 nm. In order to tap a comb spectral reference for the linearization of the sinusoidal modulation signal, the output signal from the FDML wavelength-swept laser is divided by a 99:1 directional coupler. For simultaneous detection, 99% of the source proceeds to the FBG array and the other 1% goes to the PMF Sagnac interferometer. The main portion of laser output passes through a circulator and is launched into the sensor array.

As seen in figure 1, the broadband light at the input port travels into the 50:50 coupler and splits into two counter-propagating beams by a 50:50 power ratio. A fiber Sagnac interferometer based on a PMF is used to generate a comb-fringe spectrum, as shown in the dashed box of figure 1. The comb spacing $\Delta\lambda_{\text{peak-peak}}$ is inversely proportional to the length and birefringence of the PMF, as follows:

$$\Delta\lambda_{\text{peak-peak}}=\frac{\lambda^2}{\Delta n_{\text{eo}}L} \quad (1)$$

where λ is the operating wavelength, Δn_{eo} is the birefringence and L is the effective length of the PMF [19]. Assuming the PMF has the following parameters, L = 140 cm, λ = 1540 nm, Δn_{eo} = 0.000 38, each comb-fringe peak is separated by $\Delta\lambda_{\text{peak-peak}} \approx 4.5$ nm. Four periods are monitored within the operating range of this FDML wavelength-swept laser.

For the characterization of the FDML wavelength-swept laser source, the transmission spectrum of the interferometer can be monitored using two different detection methods: the optical spectrum analyzer (OSA from Agilent Co.) and the voltage response of the photo-detector (PD, New Focus, 1817-FC) 1, shown in figures 2(a) and (b), respectively. From the peak hold mode OSA spectrum, it is easily confirmed that all of the comb spacings among the peaks B, D, F and H and the troughs A, C, E, G and I are uniform and almost the same at 4.5 nm (figure 2(a)). It appears that both edges of the spectral height are exaggerated to show higher intensities than the other inner center spectral region. This is a consequence of the accumulated acquisition-time error of the peak hold mode in the OSA, because the sinusoidal wave stays relatively longer in the edge spectral region than in the center spectral region. This distortion can be easily ignored because the spectral height will not influence the value of the comb spacing of the absolute wavelength. Therefore, the spectral information of the absolute wavelength can be used as a comb spectral reference for the linearized interrogation.

Conversely, the spectral information can be simultaneously obtained using the voltage variation from PD 1 with respect to the scanning time into the FFP-TF, which is used for the real-time interrogation of the FBG response. As shown in figure 2(b), the time-encoded parameter, $\Delta\tau$, is not uniform on the time axis of μs. Based on detailed monitoring, it is clear that the comb spacing around the center spectral region, such as C′ to E′ and E′ to G′, is relatively closer than the spacing around the edge spectral regions, such as A′ to C′ and G′ to I′. The distortion of comb spacing has a strong, critical influence on the performance of the FBG sensor system, owing to the nonlinear response in converting the time-encoded parameter, $\Delta\tau$, into the absolute wavelength position of the FBGs.

For the linearization of figure 2(b), a one-to-one comparison is performed between the absolute wavelength of points A–I of figure 2(a) and the time-encoded parameter of points A′–I′ of figure 2(b), which are the respective peaks and troughs of the comb-fringe spectra. Couplings of six points are used for obtaining the coefficients of the polynomial equation. From the corresponding coupling of these six points, a simple polynomial equation between those two parameters can be obtained. To linearize the time-encoded parameter, we use the third-order polynomial equation. Equation (2) is the third-order polynomial conversion relation, where the output of λ is the absolute wavelength measured with the OSA, and the input of $\Delta\tau$ is the time-encoded parameter measured with PD 1:

$$\lambda=1533.7-2.510\,65\times10^{-1}[\Delta\tau]+1.192\,3104\times10^{-1}[\Delta\tau]^2-3.072\,464\times10^{-3}[\Delta\tau]^3. \quad (2)$$

It is certain that all of the time-encoded parameter points can correspond to the absolute wavelength parameters by this relation, as seen in figure 3(*a*). With the specific laser condition, this process is only needed a single time. The empirical relation of equation (2) can be modified for each different FDML laser condition, such as for swept speed or gain bandwidth. Around the center spectral region in figure 3(*a*), the relationship of both parameters is approximately linear, but becomes very nonlinear at both the edge spectral regions. Such nonlinearity is caused by the sinusoidal modulation of the FFP-TF.

Since the distortion relation can be specified numerically, it can also be used to induce inverse linearization from the time-encoded parameter, $\Delta\tau$, into the new axis of the wavelength-encoded parameter, which can be defined as $\Delta\lambda$. Figure 3(*b*) shows the relationship between the absolute wavelength, λ, and the new axis of $\Delta\lambda$ obtained by the inverse polynomial conversion. From the perfectly linear plot of figure 3(*b*), we confirmed that the time-encoded parameter of $\Delta\tau$ from PD 1 is linearly converted to the wavelength-encoded parameter of $\Delta\lambda$.

Experimentally, the conversion equation can be numerically induced in real-time using a LabVIEW program and comb-fringe spectrum data obtained using a high speed PD 1 and a data acquisition board. Then, we can directly adapt the conversion process from the time-encoded parameter from PD 2 to the wavelength-encoded parameter of $\Delta\lambda$, for a uniform wavelength-spacing FBG sensing signal in real-time.

Based on the calibration method, the linearization of the FBG response has been demonstrated experimentally (figure 4). Figure 4(*a*) shows the reflected laser spectrum from the array of four FBGs, which was detected by the voltage response of PD 2 along the time-encoded parameter of FFP-TF scanning. It is clear that the two edge peaks show a relatively broad linewidth compared with the other two center peaks (broader in the case of the right edge), and this distortion results from the sinusoidal modulation with nonlinear response time. As the signal goes farther from the center region, the linewidth broadens and the peak location moves to an imprecise position. The inset figure shows the OSA measurement with respect to the absolute wavelength, demonstrating that the four lasing peaks have a similar line-width without distortion. Based on the third-order polynomial conversion process, we successfully obtain the linearized reflection spectrum of the four FBGs with respect to the wavelength-encoded parameter, $\Delta\lambda$, as shown in figure 4(*b*). It is also clear that the reflected linewidths of the FBGs are similarly narrowed along all regions of the center and both edges, in comparison with those shown in figure 4(*a*).

Space ratios between each of the FBGs are the same in cases of OSA measurement and wavelength-encoded parameter. If we take the ratio between FBG1 and FBG4 to be 1, the measured ratios between neighboring signals are 0.54, 0.22 and 0.24, respectively, for both cases. However, in the case of the time-encoded parameter in figure 4(*a*), the measured ratios are 0.51, 0.17 and 0.32, respectively, owing to the filter scan speed in the center wavelength region. This means that the entire scanning region is successfully linearized for uniform wavelength spacing, after calibration.

For a practical demonstration of the FBG interrogation, we applied a static strain up to 3.2 mε (with a small step of 200 $\mu\varepsilon$, repeated 16 times) at one of the FBGs, $\lambda = 1550.06$ nm. This wavelength is a nonlinear response region of the sinusoidal modulation signal, as shown in figure 3(*a*). Figure 5 shows the reflected laser spectra of the FBGs with respect to the static strain. As the center wavelength of the reflected laser peak is shifted to the edge region, the linewidth broadens and the peak interval widens, as shown in figure 5(*a*). However, when the *x*-axis is calibrated into the wavelength-encoded parameter of uniform spacing in figure 5(*b*), the reflected linewidths are narrow, separated evenly and shifted

linearly. In addition, the total wavelength shift caused by strain is 3.23 nm (15% of the whole wavelength scanning region of 23 nm), the same as the OSA measurement. The inset of figure 5(*b*) shows the OSA measurement with respect to the absolute wavelength. It is shown that both linewidths and the total wavelength scan behavior are totally linearized after calibration. In addition, figures 6(*a*) and (*b*) represent the strain relationships with respect to the time-encoded parameter and the wavelength-encoded parameter, respectively. The wavelength-encoded parameter, $\Delta\lambda$, varies linearly in figure 6(*b*), but the time-encoded parameter, $\Delta\tau$, varies nonlinearly, especially at longer wavelengths or edge regions, in figure 6(*a*). The curved point pattern shown in figure 6(*a*) is closely related to the nonlinear response shown in figure 3(*a*). The lines of figure 6 indicate the first-order fitting of these measurement points. The fit-slope coefficient of figure 6(*a*) was determined to be $1.24 \pm 0.032 \ \mu\text{s m}\varepsilon^{-1}$, and the fit-slope coefficient of figure 6(*b*) was determined to be 1.08 ± 0.001 39 nm $\mu\varepsilon^{-1}$. Hence, the fit variation of the time-encoded parameter, 2.58%, can be drastically decreased to 0.13% for the wavelength-encoded parameter.

4. Conclusions

Based on the comb spectral reference of the PMF Sagnac interferometer, we have induced a new uniform spacing axis of the wavelength-encoded parameter, $\Delta\lambda$, to solve the non-uniform temporal response due to the sinusoidal wave modulation. This real-time calibrated interrogation system improves the sensing accuracy for most of the broad wavelength scanning region, including both edges. The novel development of an improved linear response, in addition to a higher speed over several tens of kHz, is practically important for wide application of the FBG sensor system with the FDML wavelength-swept laser.

Acknowledgments

References

1. Kersey AD, Davis MA, Patrick HJ, LeBlane M, Koo KP, Askins CG, Putnam MA, Friebele EJ. Fiber grating sensors. J Lightwave Technol. 1997; 15:1442.

2. Bang HJ, Jun SM, Kim CG. Stabilized interrogation and multiplexing techniques for fibre Bragg grating vibration sensors. Meas Sci Technol. 2005; 16:813.

3. Kim CS, Lee TH, Yu YS, Han YG, Lee SB, Jeong MY. Multi-point interrogation of FBG sensors using cascaded flexible wavelength-division Sagnac loop filters. Opt Express. 2006; 14:8546. [PubMed: 19529233]

4. Chung S, Kim J, Yu BA, Lee B. A fiber Bragg grating sensor demodulation technique using a polarization maintaining fiber loop mirror. IEEE Photonics Technol Lett. 2001; 13:1343.

5. Song M, Yin S, Ruffin PB. Fiber Bragg grating strain sensor demodulation with quadrature sampling of a Mach–Zehnder interferometer. Appl Opt. 2000; 39:1106. [PubMed: 18337990]

6. Yun SH, Richardson DJ, Kim BY. Interrogation of fiber grating sensor arrays with a wavelength-swept fiber laser. Opt Lett. 1998; 23:843. [PubMed: 18087360]

7. Jung EJ, Kim CS, Jeong MY, Kim MK, Jeon MY, Jung WG, Chen Z. Characterization of FBG sensor interrogation based on a FDML wavelength swept laser. Opt Express. 2008; 16:16552. [PubMed: 18852764]

8. Nakazaki Y, Yamashita S. Fast and wide tuning range wavelength-swept fiber laser based on dispersion tuning and its application to dynamic FBG sensing. Opt Express. 2009; 17:8310. [PubMed: 19434164]

9. Chen D, Fok MP, Shu C, He S. Fiber Bragg grating interrogation for a sensing system based on a continuous-wave Fourier domain mode locking fiber laser. Proc CLEO/QELS 2008. 2008; 5 CMJ.

10. Kim DG, Yoo W, Swinehart P, Jiang B, Haber T, Mendez A. Development of an FBG-based low temperature measurement system for cargo containment of LNG tankers. Proc SPIE. 2007; 6770:67700D.

11. Wu MC, Prosser WH. Simultaneous temperature and strain sensing for cryogenic applications using dual-wavelength fiber Bragg gratings. Proc SPIE. 2003; 5191:208.

12. Eigenwilling CM, Biedermann BR, Palte G, Huber R. K-space linear Fourier domain mode locked laser and applications for optical coherence tomography. Opt Express. 2008; 16:8916. [PubMed: 18545605]

13. Vergnole S, Levesque D, Bizheva K, Lamouche G. Optimal signal processing of nonlinearity in swept-source and spectral-domain optical coherence tomography. Appl Opt. 2012; 51:1701. [PubMed: 22505160]

14. Hu Z, Rollins AM. Fourier domain optical coherence tomography with a linear-in-wavenumber spectrometer. Opt Lett. 2007; 32:3525. [PubMed: 18087530]

15. Wu T, Ding Z, Wang L, Chen M. Spectral phase based k-domain interpolation for uniform sampling in swept-source optical coherence tomography. Opt Express. 2011; 19:18430. [PubMed: 21935211]

16. Kim CS, Han YG, Kang JU, Choi B, Nelson JS. Polarization-insensitive multi-wavelength switching based on polarization-selective long-period fiber gratings. Opt Express. 2004; 12:6082. [PubMed: 19488249]

17. Kim CS, Kang JU. Multi-wavelength switching of Raman fiber ring laser incorporating composite PMF Lyot–Sagnac filter. Appl Opt. 2004; 43:3151. [PubMed: 15176205]

18. Kim DH, Kang JU. Sagnac loop interferometer based on polarization maintaining photonic crystal fiber with reduced temperature sensitivity. Opt Express. 2004; 12:4490. [PubMed: 19484000]

19. Lee TH, Lee HD, Kim CS, Jeong MY. Characterization of variable reflectivity of a polarization-maintaining fiber Sagnac mirror for long-distance remote fiber Bragg gratings cavity sensors. Meas Sci Technol. 2010; 21:115303.
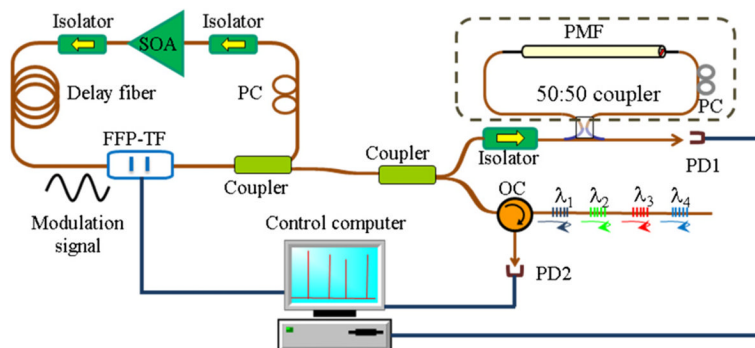
Figure 1.
Experimental setup for the linearized interrogation of an FBG sensor system based on an FDML wavelength swept laser. The dashed box shows a PMF Sagnac interferometer for the calibration signal. SOA: semiconductor optical amplifier, FFP-TF: fiber Fabry–Perot tunable filter, PC: polarization controller, PMF: polarization maintaining fiber, PD: photo-detector, OC: optical circulator.
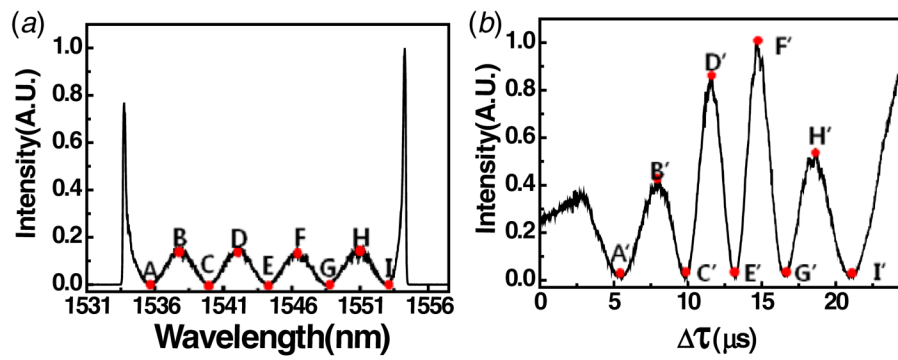
Figure 2.
(*a*) Spectrum of a PMF Sagnac interferometer in the OSA. (*b*) Spectrum of a PMF Sagnac interferometer in PD 1.
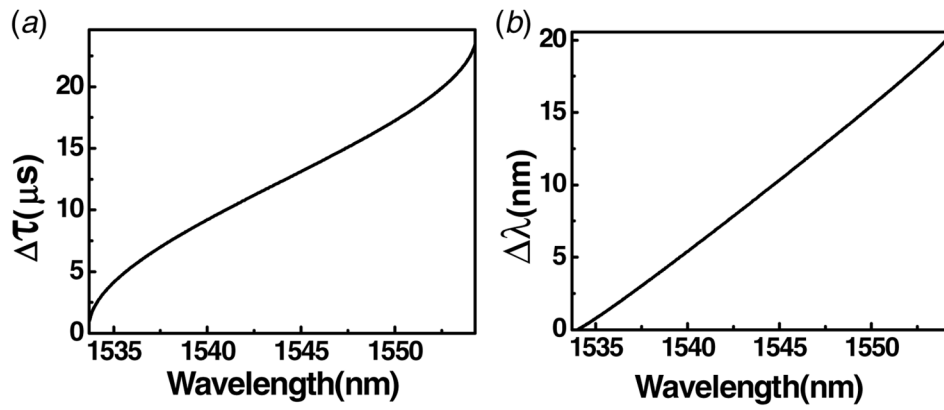
Figure 3.
(*a*) Original response of the time-encoded parameter, $\Delta\tau$, with respect to absolute wavelength. (*b*) Converted response of the wavelength-encoded parameter, $\Delta\lambda$, from polynomial equation.
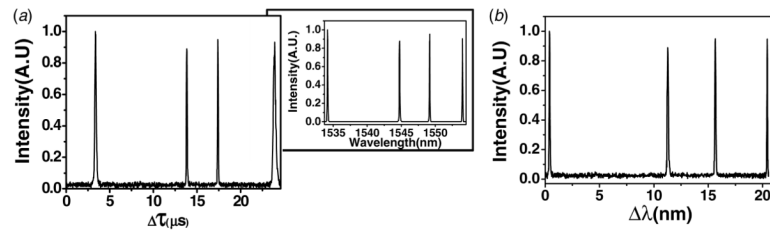
Figure 4.
(*a*) Distorted reflection spectrum of FBG sensors with respect to the time-encoded
parameter. The inset shows the OSA measurement with respect to the absolute wavelength.
(*b*) Linearized reflection spectrum of FBG sensors with respect to the wavelength-encoded
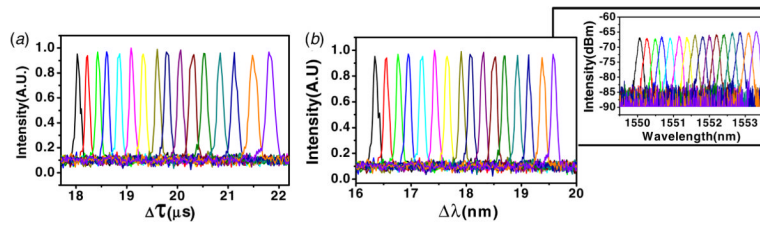parameter.

Figure 5.
(*a*) Strain response of an FBG sensor with respect to the time-encoded parameter, (*b*) linearized strain response of an FBG sensor with respect to the converted wavelength-encoded parameter. The inset shows the OSA measurement with respect to the absolute wavelength.
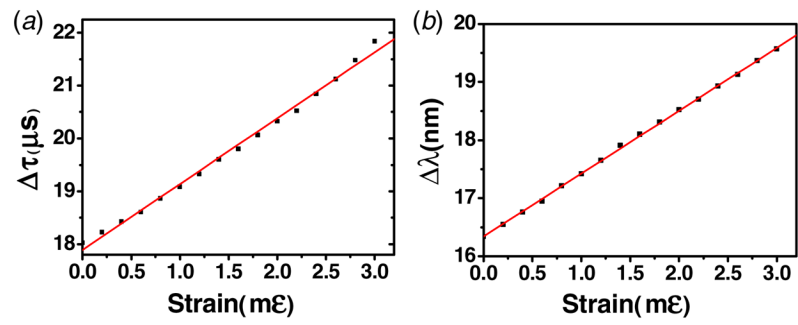
Figure 6.
Strain response of an FBG sensor: (*a*) with respect to the time-encoded parameter, (*b*) with respect to the converted wavelength-encoded parameter.